Hindawi
International Transactions on Electrical Energy Systems
Volume 2022, Article ID 9374638, 14 pages
https://doi.org/10.1155/2022/9374638

Research Article

A Grid-Connected Solar PV/Wind Turbine Based Hybrid Energy System Using ANFIS Controller for Hybrid Series Active Power Filter to Improve the Power Quality

Pazhanimuthu Cholamuthu,[1] Baranilingesan Irusappan,[1] Suresh Kalichikadu Paramasivam,[2] Senthil Kumar Ramu,[2] Suresh Muthusamy,[3] Hitesh Panchal,[4] Ramakrishna S S Nuvvula,[5] Polamarasetty P Kumar,[5] and Baseem Khan[6]

[1]*Department of Electrical and Electronics Engineering, KPR Institute of Engineering and Technology, Coimbatore, Tamil Nadu, India*
[2]*Department of Electrical and Electronics Engineering, Sri Krishna College of Technology, Coimbatore, Tamil Nadu, India*
[3]*Department of Electronics and Communication Engineering, Kongu Engineering College, Perundurai, Erode, Tamil Nadu, India*
[4]*Department of Mechanical Engineering, Government Engineering College, Patan, Gujarat, India*
[5]*Department of Electrical and Electronics Engineering, GMR Institute of Technology, Rajam 530049, India*
[6]*Department of Electrical and Computer Engineering, Hawassa University, Hawassa, Ethiopia*

Correspondence should be addressed to Baseem Khan; baseem_khan04@yahoo.com

Received 16 June 2022; Revised 12 July 2022; Accepted 20 September 2022; Published 14 November 2022

Academic Editor: Ravi Samikannu

The current needs of more nonlinear loads and the frequent usage of single-phase loads in three-phase system drastically create power quality issues in the grid-connected system. As a consequence, it creates an undesirable power quality issue (PQI) in the form of a change in the nature of voltage and current magnitude and waveforms in the power system. The voltage-related PQI leads to a huge disturbance in the system when compared with the current-related PQI. The hybrid series active power filter provides grids with the required voltage in series and suppresses the voltage-related harmonics caused by grid-connected nonlinear loads. The present work deals with an adaptive neurofuzzy inference system controller for the generation of a reference voltage signal that uses a reduced active filter rating. The simulation study was done in the MATLAB 2020b/Simulink environment and the experimental effectiveness of the proposed ANFIS controller was compared with that of a conventional controller. In the grid-connected system, this system prevents voltage quality problems such as voltage sag, flickering, voltage swell, neutral currents, and reactive power. The renewable energy sources interfaced into the DC-link minimize short and long voltage challenges so that they improve the overall performance of the system. In accordance with IEEE standard 519-1992, a prototype model was proved to demonstrate that the power delivery system works effectively under different conditions and reduces the total harmonic distortion by approximately 30%, which is less than the 5% acceptable limit.

1. Introduction

The major usage of nonlinear loads like electronic ballasts, SMPS, rectifiers, inverters, battery chargers, single-phase diode bridge rectifiers, power converter-fed drives, arc welding, furnaces, uninterrupted power supply, adjustable-speed drive, diode bridge rectifier, thyristor converter, and consumer electronics is producing an unnecessary power quality (PQ) disturbance in the grid-connected system [1–3]. In addition to fluctuations, voltage dips, oscillatory transients, momentary interruptions, harmonic resonance, harmonics, and other issues related to PQ, these loads also

cause significant power budget blowouts. Similarly, single-phase load usage in a three-phase system generates unbalanced current and neutral current in the system, generating inefficient voltage regulation, extreme neutral current, excessive reactive power, and load unbalancing [4,5] formalized paraphrase. An increase in harmonics in the power system has several negative effects, including additional heating, amplifying harmonics due to banks of power factor correction capacitors, reducing transmission system efficiency, distribution transformers' overheating and defective electronic equipment, incorrect operation of circuit breakers, creating errors in measuring equipment, and communication and control signal interference. Poor power quality leads to production loss in industries, life-threatening consequences in hospitals, loss of critical communication in airports, and so on [6–8]. In a country, poor power quality causes a loss in overall productivity, which will badly affect its economy. Numerous studies have been conducted on the solutions to PQ problems such as passive filters (PF), active filters (AF), hybrid filters (HF), and custom power devices. Harmonic-related problems in the electrical power supply can be resolved simply, moderately, and reasonably with a PF [7–10]. However, PFs have shortcomings such as their size, complexity in filter design, resonance, and tuning problems. When compared with passive approaches, active filtering approaches for PQ enhancement have proven to be more effective because of their quicker response time, smaller size, and superior performance in recent years. Furthermore, active filtering automatically adjusts to changes in network characteristics, reducing the possibility of resonance between the filter and the network impedance [11–15]. A problem with AFs is that they produce high-frequency noise when high currents are switched on and off rapidly, which can cause electromagnetic interference in a power system distribution. A hybrid power filter (HPF) is formed by combining the operations of PFs and an active power filter (APF), and it alleviates the problems associated with the individual operation of active and passive filtering [11,13,16–20].

There are many controllers proposed for HSAPF in the literature, but they are limited to certain difficulties. Traditional controllers have some difficulties compensating for long-term system issues [21–23]. To achieve system performance improvements, neural networks and fuzzy logic are combined as a controller. To generate harmonic compensating voltage, an Adaptive Neurofuzzy Inference System (ANFIS) implemented controller is used. Calculations of reference current are to be carried out continuously as the load on the system changes from moment to moment. It is proposed to implement an ANFIS-based digital processor that generates the gating signals for thyristors in the adaptive shunt passive filter, as well as PWM signals for switching devices in the SAPF [24–26]. The modified p-q controller is the main controller to tune the parameters of active and reactive power. This can be done through ANFIS to achieve voltage profile improvement in the system. In order to compensate for the harmonic and the reactive power requirements of the nonlinear load, it produces the appropriate compensation signals for the active filter [27–31]. It also adjusts the passive filter component values. Using tap-changing transformers or uninterruptible power supplies as traditional methods for suppressing voltage variations has the disadvantage of being bulky, expensive, and slow enough to allow voltage sag effects at the load side to be eliminated. Due to its high controllability and reliability, the Hybrid Series Active Power Filter (HSAPF) uses a voltage source inverter (VSI) as an active filter in series and in parallel with a shunt high-pass filter. The problem of long-term interruptions or block-outs in the supply system is eliminated by incorporating renewable energy sources (RES) into the DC-link. The system improves performance and lowers the THD level below 5% as required by IEEE standard [32–36]. The purpose of this study is to propose an HSAPF to address power quality issues associated with voltage in grid-connected systems with the integration of renewable energy sources (RES). Thus, in this research, the HSAPF is proposed as a compensatory measure for power quality issues in RES integrated grid-connected systems.

2. System Description

2.1. Configuration of SAPF. The SAPF injects harmonic voltages to or from the source voltage as the voltage waveform is transmitted across the nonlinear load. During fundamental component operation, the device presents zero resistance. However, for harmonic component operation, it appears as a resistance with a high impedance. LC filters containing one or more single-tuned elements with or without a high-pass filter make up shunt passive filters. The SAPF with a shunt PF called HSAPF operates as a high impedance harmonic isolator. This is done by injecting a controlled harmonic voltage source between the nonlinear load and the source as shown in Figure 1. The result is that all load current harmonics except those at fundamental frequency are restricted to the passive filter. The load current harmonics are reduced by separating the source from the load.

Grid harmonic currents are not compensated, so instead they act as high impedance currents for loads. Thus, the passive filter can be located on the customer side of the system so that harmonic currents from the power system will not be consumed. In this case, there is no harmonic resonance, and the supply does not have a harmonic flow. HSAPF incorporates the features of a passive high-pass filter, thereby bypassing all upper order harmonics, while SAPF compensates for low order harmonics in the supply voltage.

2.2. The Proposed System Description. It is proposed that photovoltaic and wind energy systems use common DC-link combined with shunt passive filters while nonlinear loads are linked to standard voltage and current harmonic sources. SAPFs reduce the harmonic components of voltage waveforms by injecting voltage components into series with the supply voltage. It is a way to prevent voltage imbalances, voltage sags, and swells resulting from load fluctuations.

The two major RES are integrated into the system in two places, namely, the main source and, secondly, a source for

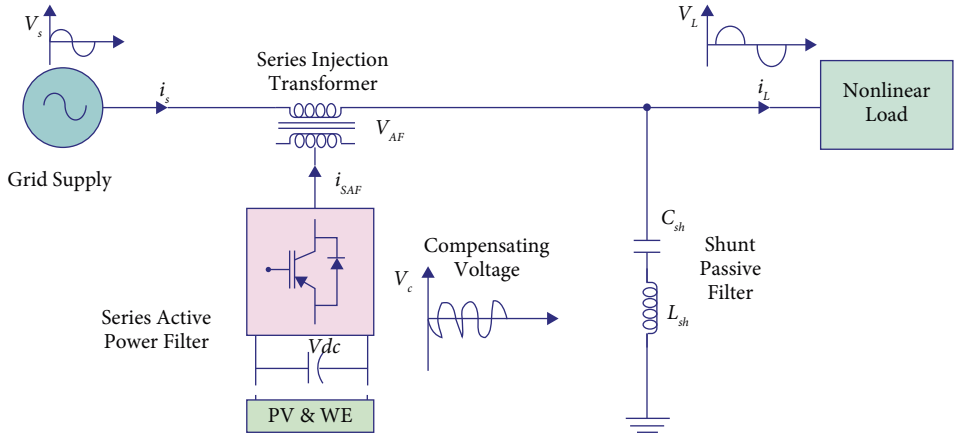

Figure 1: Basic configuration of Hybrid Series Active Power Filter.

compensation of long power interruptions through the DC-link. Boosting the low voltage output voltage of the PV panels is achieved by connecting the solar array to a DC-DC boost converter. Several methods for tracking maximum power points (MPPT) have been discussed in the literature, among which incremental conductance (IC) and perturbation and observation (P&O) are commonly employed. Here, the P&O model is used as it utilizes a simple feedback model and fewer parameters compared to the IC, which spends more time tracking maximum power. This algorithm is used to achieve the optimal solar panel output power from the solar energy source. A solar battery bank stores excess power generated by the panels, and the charge controller converts this energy into AC power.

A system that produces wind power is made up of a multipole synchronous generator attached to an adjustable-speed wind turbine. With the help of the rectifier, the output of a three-phase voltage is transformed into a DC voltage. Despite the deviation in the rectified DC voltage, the rectifier's output is combined with a DC-DC buck-boost converter to maintain a constant DC voltage. The output voltage of the rectifier is kept constant even when rectified DC voltage varies because its output is coupled to a DC-DC buck-boost converter. The maximum power of the converter was measured successfully with an MPPT technique by determining the ratio of efficiency to turbine speed.

With a series injection transformer, SAPF injects the compensating voltage in parallel with the voltage supply. Figure 2 illustrates the DC-link voltage generation process using photovoltaic (PV) and wind energy (WE) photovoltaic systems. SAPF is an inverter that uses a VSI made up of transistors and DC-link capacitors, and its compensation is largely influenced by the amount of energy available in the DC-link. This allows a reference value to be set for the DC-link capacitor voltage. A change in the load situation can result in a change in the power balance between the load and the source. SAPF will be able to compensate for variations in real power by using DC-link interfaced RES. This is achieved by injecting the harmonic compensating voltage through an injection transformer in series with the power supply voltage. Through the integration of renewable energy sources into the DC-link, the HSAPF can ensure consistent supply over the long term. The availability of RES in the DC-link in the system causes different kinds of operation to occur in the system, as shown in Table 1.

3. Design Parameters

The inductor (L_s) power and the capacitor C supplied current (i_s) accumulated in the inductor are expressed in terms of voltage across inductor as

$$xV_L = L_s \times \frac{di_s}{dt}. \tag{1}$$

The boost converter's inductor value is determined from the following expression:

$$L = \frac{V_{in} \times D \times T}{\Delta I}, \tag{2}$$

where D, V_{in} ΔI, T are the duty cycle, input voltage, inductor ripple current, and time period, respectively.

As a result of the converter, the average output voltage equals

$$V_{\text{out}} = \frac{V_{\text{in}}}{1 - D}. \tag{3}$$

To maximize wind energy output, a buck-boost converter is connected to PMSG through MPPT techniques. The maximum output voltage of V_m in the line-line voltage of rms value is expressed as

$$V_{rms} = \frac{\sqrt{3}V_m}{\sqrt{2}}. \tag{4}$$

When the buck-boost converter steps up or down after rectification, the voltage is expressed as

$$V_{dc} = -\frac{D}{1 - D} \times V_{dcrx}. \tag{5}$$

The SAPF is designed to restore a certain amount of power when the system supply sags. For a 3.120 kVA load, the following sizing may be recommended. This is in order to reduce 65% voltage sag, while simultaneously compensating the harmonics in the source current and maintaining power factor.

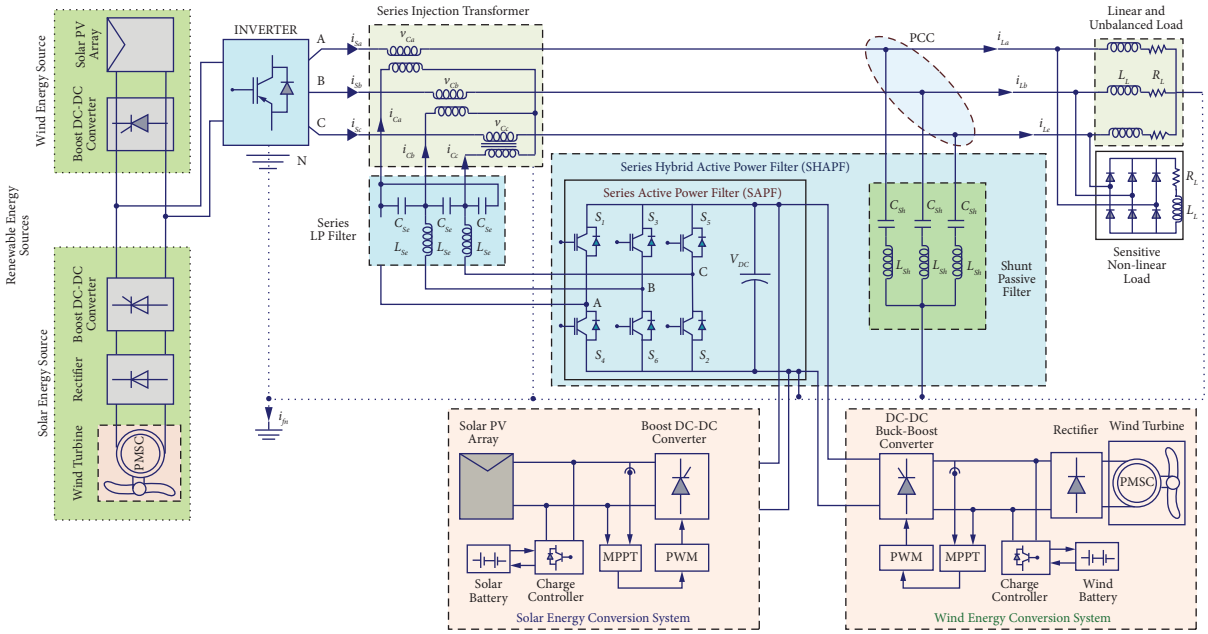

Figure 2: Topology of the proposed grid-integrated hybrid system.

Table 1: Operating modes of the proposed system.

Mode	Available source	Voltage condition	Power	Operation of energy sources in DC-link
Mode 1	PS = 1 PW = 0 PBS = 0 PBW = 0	VBS ≤ VBS, Min VBW ≤ VBW, Min or VS = 0	PS ≥ PL and PW < PL or PW = 0	The SAPF utilizes solar energy to compensate for harmonics, reactive power, and share load demand when solar power is superior to load demand.
Mode 2	PS = 1 PBS = 1 PW = 0 PBW = 0	VBS ≥ VBS, Min VBW ≤ VBW, Min or VS = 0	PS ≥ PO and PW < PL or PW = 0	Having a fully charged battery and a solar array that can supply power to both the DC-link and the load at once, the SAPF is able to run at maximum efficiency. During solar battery charging, constant voltage is switched off to prevent self-discharge.
Mode 3	PS = 0 PW = 0 PBW = 0 PBS = 1	VBS ≥ VBS, Min VBW ≤ VBW, Min or VS = 0	PS < PL or PS = 0 and PW < PL Or PW = 0	Power is supplied to the SAPF-PV load and DC-link when the battery is fully charged.
Mode 4	PS = 0 PBS = 0 PBW = 0 PW = 1	VBS ≤ VBS, Min VBW ≤ VBW, Min or VS = 0	PS < PL or PS = 0 and PW ≥ PL	SAPF-WE compensates for harmonics and reactive power when generating wind energy exceeds load demand, as well as sharing load demands when the solar and wind batteries are not fully charged.
Mode 5	PS = 0 PBS = 0 PW = 1 PBW = 1	VBS < VBS Min VBW ≥ VBW, Min or VS = 0	PS < PL or PS = 0 and PW = 0	As a result of fully charging the wind battery, the SAPF-WE can operate simultaneously on both DC-link and load power from the wind turbine. To prevent self-discharge, continuous voltage charging is switched off for the wind battery.
Mode 6	PS = 0 PW = 0 PBS = 0 PBW = 1	VBS < VBS, Min VBW ≥ VBW, Min or VS = 0	PS < PL or PS = 0 and PW < PL or PW = 0	Power is provided to SAPF-WE's load and DC-link by a fully charged wind battery.

Note: PS is solar power, PW is wind power, PBS is power in solar battery, PBW is power in wind battery, VBW is voltage in wind battery, VBS is voltage in solar battery, VS is source voltage, and PL is load power.

The SAPF should have the ability for long time voltage compensation, so that backup supply is accordingly designed as $DC_{\text{source}} = 3.120 \times 65\% = 1875VA$.

The converter nominal voltage is expressed as $V_{Conv} = 1875VA/7.825A_{rms} = 239.6V_{\text{rms}}$.

The converter has the ability of transfer the rms load current and therefore the rating of converter is expressed as $I_{\text{Conv}} = I_L = 1875VA/239.6V_{\text{rms}} = 7.825A_{\text{rms}}$.

The SAPF is controlled as VSC and the DC voltage is derived as

$$v_{dc} = \left(i_{Ca}S_A + i_{Cb}S_B + i_{Cc}S_C\right)/C_{dc}. \tag{6}$$

The value of $S_1 - S_6$ is represented as converter switches and AC three-phase line voltages are v_{Ca}, v_{Cb}, and v_{Cc} expressed as

$$\begin{aligned} e_a &= v_{dc}\left(S_1 - S_2\right), \\ e_b &= v_{dc}\left(S_2 - S_3\right), \\ e_c &= v_{dc}\left(S_3 - S_1\right). \end{aligned} \tag{7}$$

The output of SAPF in volt-current equations can be expressed as

$$v_a = r_f i_{Ca} + L_f p i_{Ca} + e_a - r_f i_{Cb} - L_f p i_{Cb}, \tag{8}$$

$$v_b = r_f i_{Cb} + L_f p i_{Cb} + e_a - r_f i_{Cc} - L_f p i_{Cc}, \tag{9}$$

where r_f and L_f are value of SAPF resistance and inductance.

The SAPF compensating current is expressed as $i_{Ca} + i_{Cb} + i_{Cc} = 0$.

The current derivatives of the SAPF are obtained from the following equations:

$$p i_{Ca} = \frac{\left\{\left(v_b - e_b\right) + 2\left(v_a - e_a\right) - 3r_f i_{Ca}\right\}}{3L_f}, \tag{10}$$

$$p i_{Ca} = \frac{\left\{\left(v_b - e_b\right) + \left(v_a - e_a\right) - 3r_f i_{Ca}\right\}}{3L_f}. \tag{11}$$

The SAPF eliminates source current distortions, and only the harmonic component of load voltage is injected. Hence, the line-line fundamental component of voltage (V_{LL}) is expressed as

$$V_{LL} = \left(\frac{\sqrt{6}}{\pi}\right)V_{dc} = 0.779V_{dc}. \tag{12}$$

Here, the calculated DC-link voltage is V_{dc}.

The DC-link value is approximated to 600 V, P is power of 0.76 kVA, and T is energy storing time. Therefore, the DC-link capacitance value can be calculated as

$$C_{dc} = \frac{P \times T}{(1/2) \times V_{dc}^2} = \frac{760 \times 200 \times 10^{-3}}{(1/2) \times 600^2} = 1176\mu F \approx 2200\mu F. \tag{13}$$

Thus, the DC-link capacitance value of $2200\mu F$ is considered to be appropriate for proper voltage compensation.

4. ANFIS Controller for HSAPF

HSAPF controls the inverter by computing the reference voltage waveform for every phase, maintaining continuous DC voltage and inverter signals generation. Figure 3 demonstrates the ANFIS control scheme for the proposed HSAPF configuration. With this circuit, the reference voltage generator creates the appropriate reference voltage for the load and compensates for reactive power and harmonics generated by it. A constant DC voltage is maintained across the capacitor with this circuit.

4.1. Architecture of ANFIS Controller. ANFISs combine fuzzy approaches with neural networks (NNs) that can adapt to achieve the required performance. Integrating the characteristics of the rules, fuzzy set topology, and control system structure into an adaptive system is challenging. Due to the lack of standard techniques for turning human knowledge into rules, FLC is an essential component of the fuzzy inference system (FIS). Hence, input and output membership functions have been selected by trial and error based on the size, type, and parameters. As well, the system is limited in its adaptability due to the range of variables that are difficult to adjust. The membership functions should be tuned and the rule base should be simplified to the fewest essential rules as possible. It is proposed that the ANFIS method be used to overcome the complexity described above. NN and fuzzy qualitative approaches are combined in this method. In contrast to standard fuzzy logic, this system is trainable without the need for a lot of expert knowledge. This results in a reduced rule base.

Figure 3 shows a typical ANFIS structure with a circle indicating a fixed node and a square indicating an adaptive node. Input and output nodes are present in this structure, along with hidden layers. Acts as models and rules are contained within these layers. The MATLAB/ANFIS editor is used to generate it after the initial data from the PI controller is obtained. Observers and moderators can easily understand and modify such a feedforward multilayer system, eliminating the disadvantage. In order to simplify things, let us assume that the FIS has two inputs and one output. The Takagi-Sugeno model is based on two inputs (x and y) and an output (z) and employs a fuzzy system model in ANFIS. This system is further tuned using an error propagation-based method. The error backpropagation learning algorithm implemented on a multilayer feedforward neural network can be trained to capture the mapping implicitly.

Using the error backpropagation algorithm, the error value of instantaneous real power and reactive power is calculated by

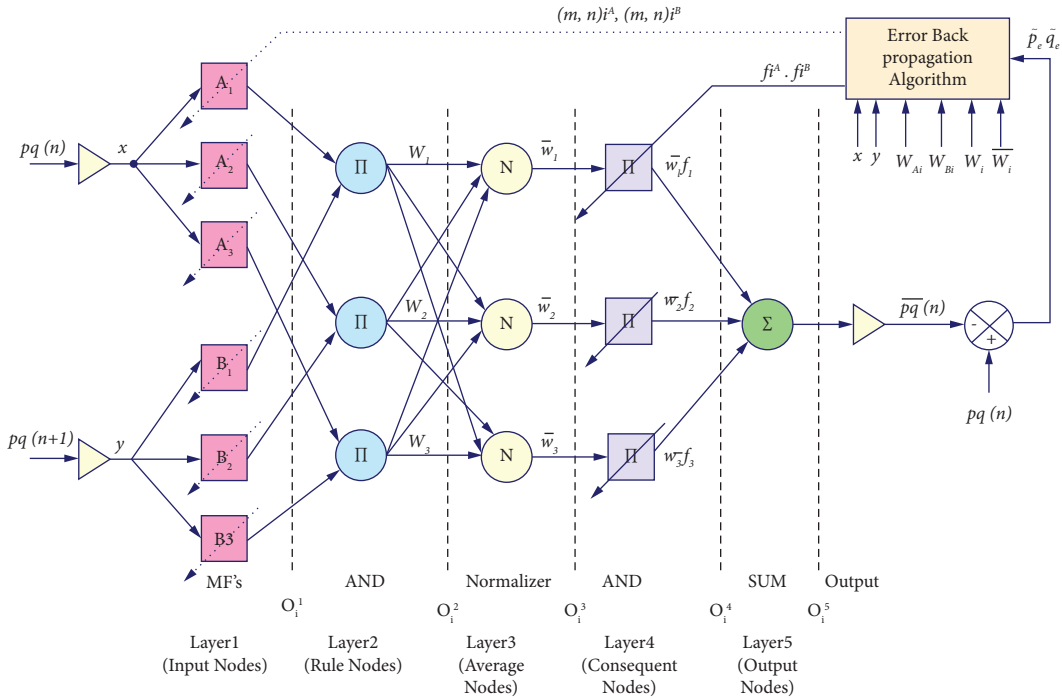

Figure 3: Schematic architecture of ANFIS controller.

$$\tilde{p} = p(n) - \overline{p}(n),$$
$$\tilde{q} = q(n) - \overline{q}(n), \tag{14}$$

$$f_1 = p_1 x + q_1 y + r_1,$$
$$f_2 = p_2 x + q_2 y + r_2, \tag{15}$$
$$f_3 = p_3 x + q_3 y + r_3,$$

$$f = \frac{W_1 f_1 + W_2 f_2 + W_3 f_3}{W_1 + W_2 + W_3} = \overline{W_1} f_1 + \overline{W_2} f_2 + \overline{W_3} f_3, \tag{16}$$

where p and q are two inputs and $\tilde{p}$ and $\tilde{q}$ are two outputs. It is possible to build up fuzzy logic rules and decide input-output membership functions using the ANFIS, a structure that can be trained using neural learning training examples. Expert knowledge can be integrated into the ANFIS as well. The IF-THEN rules of first-order constitute the basis of the connection structure. Normally, each rule takes an input variable and a constant term as its output. An IF-THEN rule set is with three fuzzy IF-THEN statements for a first-order Sugeno fuzzy model.

5. Reference Voltage Signal Estimation

For three-phase power systems with or without neutrals, instantaneous values can be used to establish the p-q theory. It covers both transient and steady state waveforms in addition to the standard voltage and current waveforms. A p-q theory is a method for computing the current and voltage components of a three-phase input voltage, based on an arithmetic transformation known as Clark's transformation, which describes how the a-b-c coordinates translate to the α-β-0 reference frame.

Calculating the SAPF instantaneous reference voltages requires a modified p-q theory. According to modified p-q theory, the source voltages are shifted by 90° when calculating instantaneous reactive power. Using LPFs and inverse transformations instead of the conventional AC components, the DC components are removed from the reference voltage before determining the compensation reference voltage.

As shown in Figure 4, the control is mainly aimed at calculating a three-phase reference compensation voltage such as v^*_{Ca}, v^*_{Cb}, and v^*_{Cc}, respectively, to compensate for distortions in the supply phase voltage such as v_{Sa}, v_{Sb}, and v_{Sc}, respectively, at the load terminals by injecting compensating voltages such as v_{Ca}, v_{Cb}, and v_{Cc} correspondingly so as to achieve full sinusoidal at PCC.

The preferred voltages at the load terminals are the supply voltage plus the injected SAPF voltage. Phase-locked loops (PLL), which synchronize with the supply voltage, are used to compensate for the distortion of the supply voltage. Voltage measurements on three phases are sensed and placed into the PLL to generate unit vectors of two quadratures (sin ωt, cos ωt). The sensed voltages from the supplies are being fed into the PLL, which is then multiplied by a suitable gain value. PLLs with discrete three-phase modes provide a frequency of 50 Hz at 50 milliseconds.

The α-β-0 reference frame voltage and current are the characteristics of the three phase supply voltages v_a, v_β, and v_0 and the three phase source currents i_a, i_β, and i_0. This filter reclaims a portion of the real power from the essential voltage component by removing the harmonic

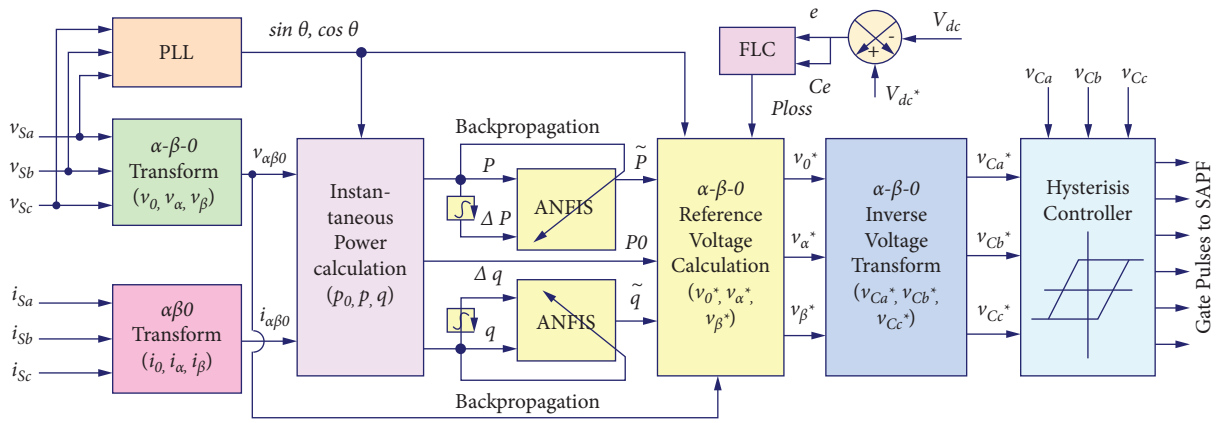

Figure 4: ANFIS-based controller for reference voltage signal generation.

components of the voltage supply. This filter regains a portion of the real power that is expressed as

$$\begin{bmatrix} v_0 \\ v_\alpha \\ v_\beta \end{bmatrix} = \sqrt{\frac{2}{3}} \begin{bmatrix} \frac{1}{\sqrt{2}} & \frac{1}{\sqrt{2}} & \frac{1}{\sqrt{2}} \\ 1 & \frac{-1}{\sqrt{2}} & \frac{-1}{\sqrt{2}} \\ 0 & \frac{\sqrt{3}}{2} & \frac{-\sqrt{3}}{2} \end{bmatrix} \begin{bmatrix} v_{sa} \\ v_{sb} \\ v_{sc} \end{bmatrix}, \tag{17}$$

$$\begin{bmatrix} i_0 \\ i_\alpha \\ i_\beta \end{bmatrix} = \sqrt{\frac{2}{3}} \begin{bmatrix} \frac{1}{\sqrt{2}} & \frac{1}{\sqrt{2}} & \frac{1}{\sqrt{2}} \\ 1 & \frac{-1}{\sqrt{2}} & \frac{-1}{\sqrt{2}} \\ 0 & \frac{\sqrt{3}}{2} & \frac{-\sqrt{3}}{2} \end{bmatrix} \begin{bmatrix} i_{sa} \\ i_{sb} \\ i_{sc} \end{bmatrix}. \tag{18}$$

The compensating voltage such as $V_{C\alpha}^*, V_{C\beta}^*$, and v_{C0}^*, respectively, in *α-β-0* reference frame is expressed as

$$\begin{bmatrix} v_{c\alpha}^* \\ v_{c\beta}^* \\ v_{co}^* \end{bmatrix} = \frac{1}{v_\alpha^2 + v_\beta^2} \begin{bmatrix} v_\alpha & v_\beta & 0 \\ v_\beta & -v_\alpha & 0 \\ 0 & 0 & v_{\alpha\beta} \end{bmatrix} \begin{bmatrix} \tilde{p} \\ \tilde{p} \\ p_0 \end{bmatrix}, \tag{19}$$

where $\overline{p}$ and $\overline{q}$ are called essential components and $\tilde{p}$and $\tilde{q}$ are called the alternating or varying element. Multiplying the compensating voltage $V_{C\alpha}^*, V_{C\beta}^*, v_{C0}^*$ in the $a-b-c$ reference frame with the expression is used to calculate the reference voltages v_{Ca}^*, v_{Cb}^*, and v_{Cc}^* in the reference frame as

$$\begin{bmatrix} v_{ca}^* \\ v_{cb}^* \\ v_{cc}^* \end{bmatrix} = \sqrt{\frac{2}{3}} \begin{bmatrix} \frac{1}{\sqrt{2}} & 1 & 0 \\ \frac{1}{\sqrt{2}} & \frac{-1}{\sqrt{2}} & \frac{\sqrt{3}}{2} \\ \frac{1}{\sqrt{2}} & \frac{-1}{2} & \frac{-\sqrt{3}}{2} \end{bmatrix} \begin{bmatrix} v_{c\alpha}^* \\ v_{c\beta}^* \\ v_{co}^* \end{bmatrix}. \tag{20}$$

Source voltages are the sum of the load voltages produced by the SAPF, and compensation voltage is represented by

$$\begin{bmatrix} v_{La} \\ v_{Lb} \\ v_{Lc} \end{bmatrix} = \begin{bmatrix} v_{Sa} \\ v_{Sb} \\ v_{Sc} \end{bmatrix} + \begin{bmatrix} v_{Ca} \\ v_{Cb} \\ v_{Cc} \end{bmatrix}. \tag{21}$$

Implementation of a modified p-q theory for a full ANFIS-based control system supports the proposed HRES-HSAPF system. Figure 5 showcases the entire system architecture of the proposed controller based HRES-HSAPF.

6. Simulation Results and Discussion

An implementation of the ANFIS-based modified PQ theory is investigated in this section to control the HSAPF DC-links through RES interfaces, and the effectiveness of this control scheme is estimated under different cases through MATLAB/Simulink. Simulation studies include three different test cases: voltage and load balanced, voltage balanced and unbalanced load, and voltage unbalanced and unbalanced load. Table 2 summarizes the simulation parameters for the RES-HSAPF system.

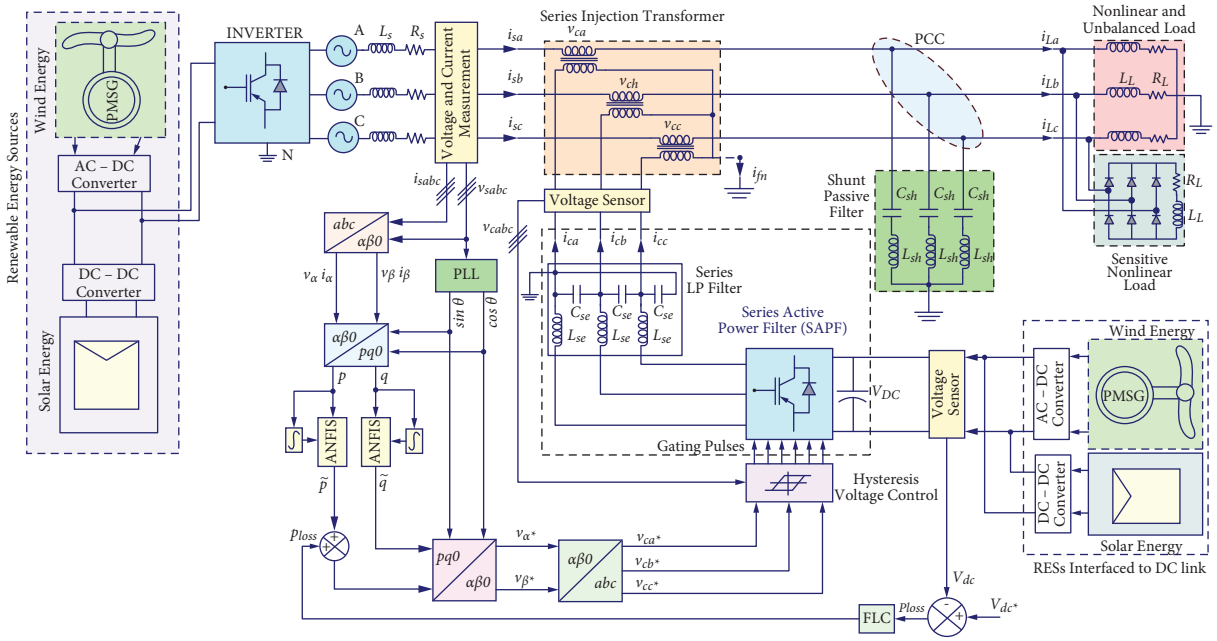

Figure 5: Overall control structure of the proposed ANFIS-based system.

Table 2: Simulation parameters of the proposed system.

Component	Parameter	Variable	Value
Source	Operating voltage	V_{ph}	240 V
	Frequency	f	50 Hz
Passive filter	LC value	C_{Se}, L_{Se}	34 μF, 12.5 mH
PV module	Number of cells	N_{cell}	6×10
	Nominal voltage	V_{nom}	12 V
	Maximum power	P_{mmp}	230 W
	Maximum voltage	V_{mmp}	35.5 V
	Maximum current	I_{mmp}	6.7 a
Wind generator	Rated power	P_w	1.20 kW
	Maximum power	P_m	1.50 kW
	Rated speed	ω_s	720 r/m
	Frequency	f	50 Hz
	Voltage	V_{ph}	240 V
DC-link	Voltage	V_{DC}	700 V
	Capacitor	C_{DC}	2200 μF
SAPF	Filter	L_S , C_S	20 mH, 80 μF
	Switching frequency	f_s	10 kHz
Series injection transformer	Controlling voltage	T_{I1} , T_{I2} , and T_{I3}	100 VA and 1 : 1100 V
PI controller	Proportional gain	K_p	6
	Integral gain	K_i	5.5
Battery bank	Nominal voltage	V_{Bat}	2×12 V
	Capacity	P_B	2×500 ah
Nonlinear load	Three-phase rectifier	R_L , L_L	10 W, 3 mH
	RL load	$R`_L$, L_L	12 W, 75 mH

As shown in Figure 6(a), the test Case 1 is initially considered voltage balanced with a balanced load and is performed for a variety of system voltage and load conditions. The proposed control structure is evaluated by applying a variety of voltage disturbances to the system. The voltage applied to the system has not changed over the period of 0 to 0.04 sec. The system is then subjected to a 25% swell in voltage between 0.04 and 0.1 sec, followed by no voltage from 0.14 to 0.14 sec. As shown in Figure 6(a), a voltage sag of 75% occurs during the same time period. No voltage injection is required from SAPF for the period from 0 to 0.04 sec. During the 0.04 to 0.1 seconds' period, a 25% voltage swell is detected. The controller compensates for it by applying a negative voltage. In other words, the SAPF injects

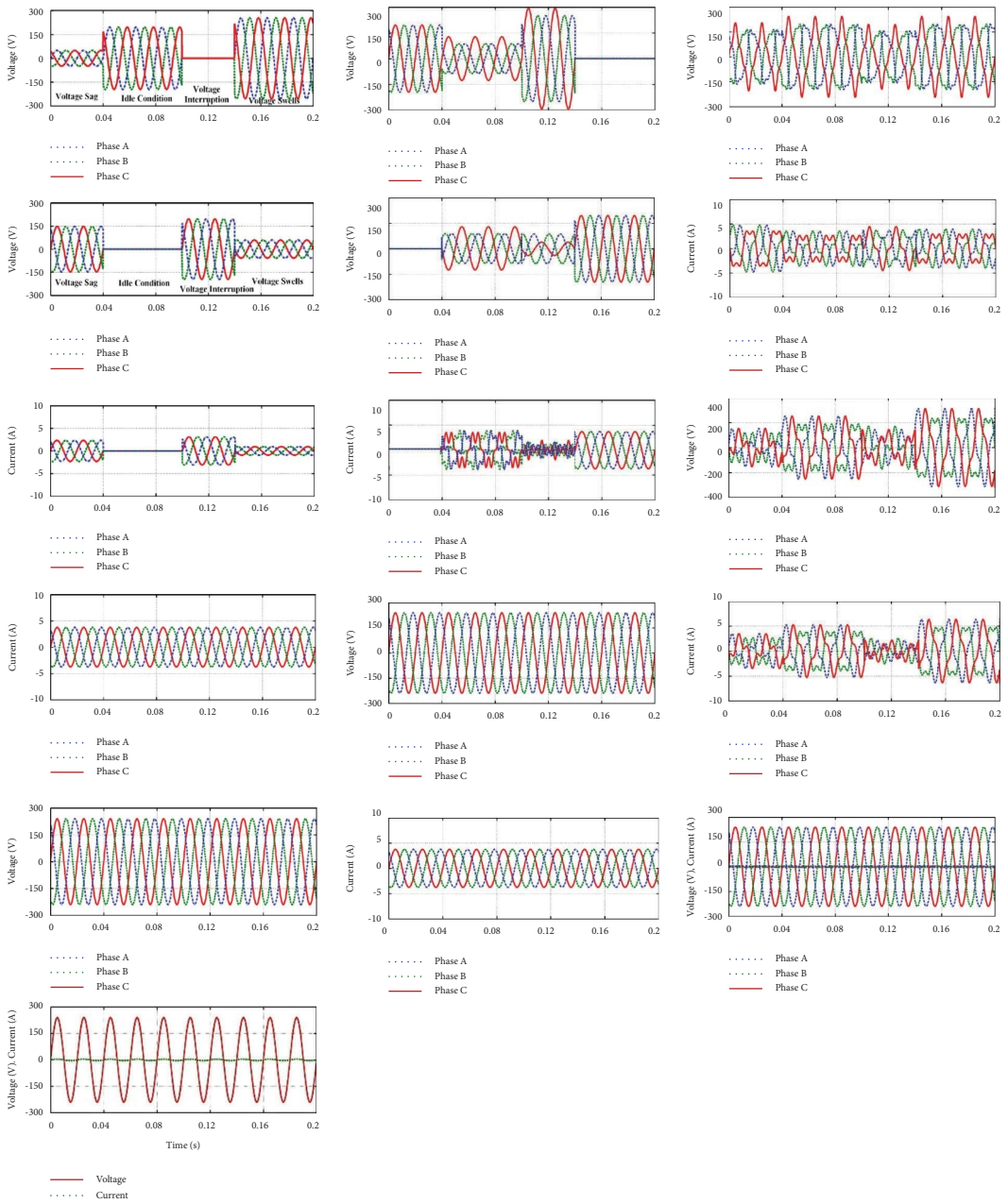

FIGURE 6: Different test cases considered for the performance analysis of the proposed controller. (a) Test Case 1. (b) Test Case 2. (c) Test Case 3.

25% of the actual 60 V through the SIT. The system voltage is interrupted for 0.1 to 0.14 sec, so compensating for the interruption requires the total nominal voltage. The SAPF injects 240 V_{rms} in series with the system at the rated system voltage. In this instance, the voltage sag occurs from 0.14 to 0.2 sec, only 25% of the nominal voltage is available, and the controller detects the remaining of 75% shortage. As a result of the switching operation of the HC, the SAPF generates the required voltage and supplies it to the SIT. A load voltage measurement is made after SAPF has performed the compensation. The modified p-q theory control scheme is applied to compensate for voltage sags, swells, and interruptions present in the system.

The test Case 2, depicted in Figure 6(b), is carried out for various system voltage and load conditions and is considered voltage balanced with an unbalanced load. Tests are performed on a single-phase load connected between two phases in this case to determine whether the load voltages are unbalanced. The controller sets the reference compensating voltage for the HC using the measured voltage prior to compensation. The voltage and current injected through the SAPF are determined by properly identifying voltage imbalances and phase angle jumps. This is to compensate for unbalanced voltage and phase angle

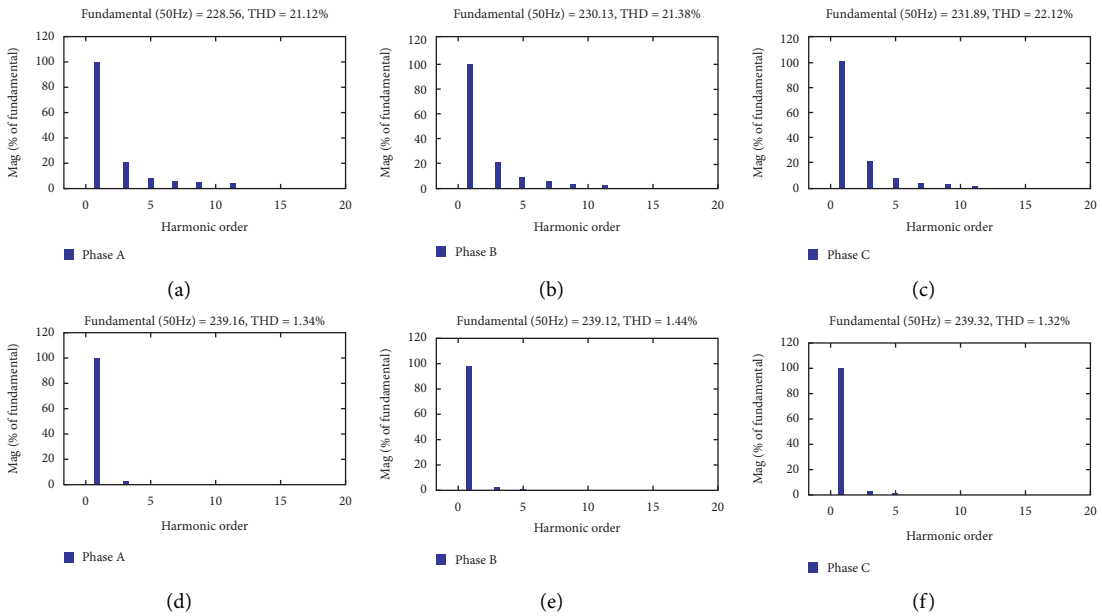

Figure 7: THD level of source current before and after compensation of the proposed controller.

jumps. A gate pulse is also generated for the SAPF via this controller. The SAPF produces the required compensating voltage based on the gate signals received. It applies the compensating voltage to the system through SIT.

Likewise, in Test Case 3, as shown in Figure 6(c), voltage unbalanced with unbalanced load is performed for various system voltage and load conditions. Under unbalanced voltages and unbalanced loads, the system performance is evaluated in test Case 3. It is assumed that the load and the system voltage are unbalanced in this test case. To verify this case, the system voltage should be generated with 5th and 7th order harmonics and the load should be operated as a single-phase unbalanced load. As the voltage imbalances between supply and load, accurate measurements of the voltages are sent to the controller. The p-q model based on ANFIS calculates the required voltage for compensation, and it is applied to the hysteresis controller to generate the necessary gating signal. The ANFIS-based modified p-q theory control scheme applied to SAPF eliminates voltage sag, voltage swell, and interruption by inserting a consistent compensating voltage in series with the supply voltage at phase angles of 0° and 180° with the purpose of decreasing voltage sag and swell. The proposed controller effectively compensates neutral currents because before compensation they have a significant number of harmonics.

In Figure 7, THD levels for three-phase source currents with the ANFIS controller before and after compensation are shown. In this case, the THD levels for three-phase source currents before and after compensating with the ANFIS controller are considered. As a result of the ANFIS controller, THD values are reduced to less than 2% after compensation.

7. Experimental Results and Discussion

A prototype of the proposed system is developed with simulated users for the evaluation of its performance: 240 Vrms, 50 Hz, three-phase, and four-wire system. To implement the control circuit, an STM32F407VGT6 is employed, which operates at 168 MHz. The floating-point unit also has the capability of processing all single-precision data types and commands of an ARM processor. The DSP and memory protection units improve application security by implementing a complete set of DSP instructions. At the PCC, the analog to digital converter acquires and interfaces voltages and source currents. Currently, the controller program calculates reference voltage signals and then compares them with carrier waves to produce gate pulses.

Three voltages and three currents are obtained with the help of six 12 bit ADC channels based on mathematical calculations of sampled data. In order to generate PWM voltage source inverters, you need to calculate and compare gate pulses required for generating reference signals and carrier waves. In order to implement the PWM VSI, six IGBTs from ST Microelectronics are used, and the IR2130 is used as a three-phase bridge driver. The controller generates six gate pulses using optical isolation before the controller connects to the IR2130, and the VSI used had a kVA rating of 1.2 kVA with a turn ratio of 1 : 1.

A set of measurements were conducted with 120 mH source inductor, 20 mH filter inductor, an 80 μF filter capacitor, and a 2200 F DC-link capacitor. The inductance and load resistance were 75 mH and 8 Ohms, respectively. IGBT inverters switch at 10 kHz. Load current and voltage are measured using AC-link voltage sensors and DC-link capacitor voltage sensors. The signal conditioning circuit of an analog to digital converter amplifies and presents the offset needed to complete the conversion. An experimental setup that tests both current and voltage harmonics generation by the SHAPF control scheme is represented in Figure 8.

A balanced sinusoidal system voltage and a balanced load are considered to evaluate the proposed controller performance. At the same time, the act of varying the voltage in the system is intended to manage voltage sags, surges, and

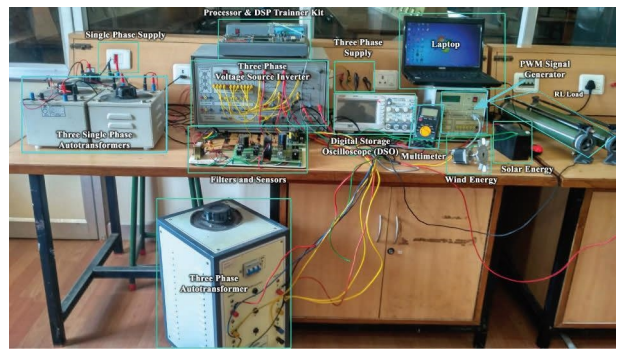

Figure 8: The proposed system experimental setup.

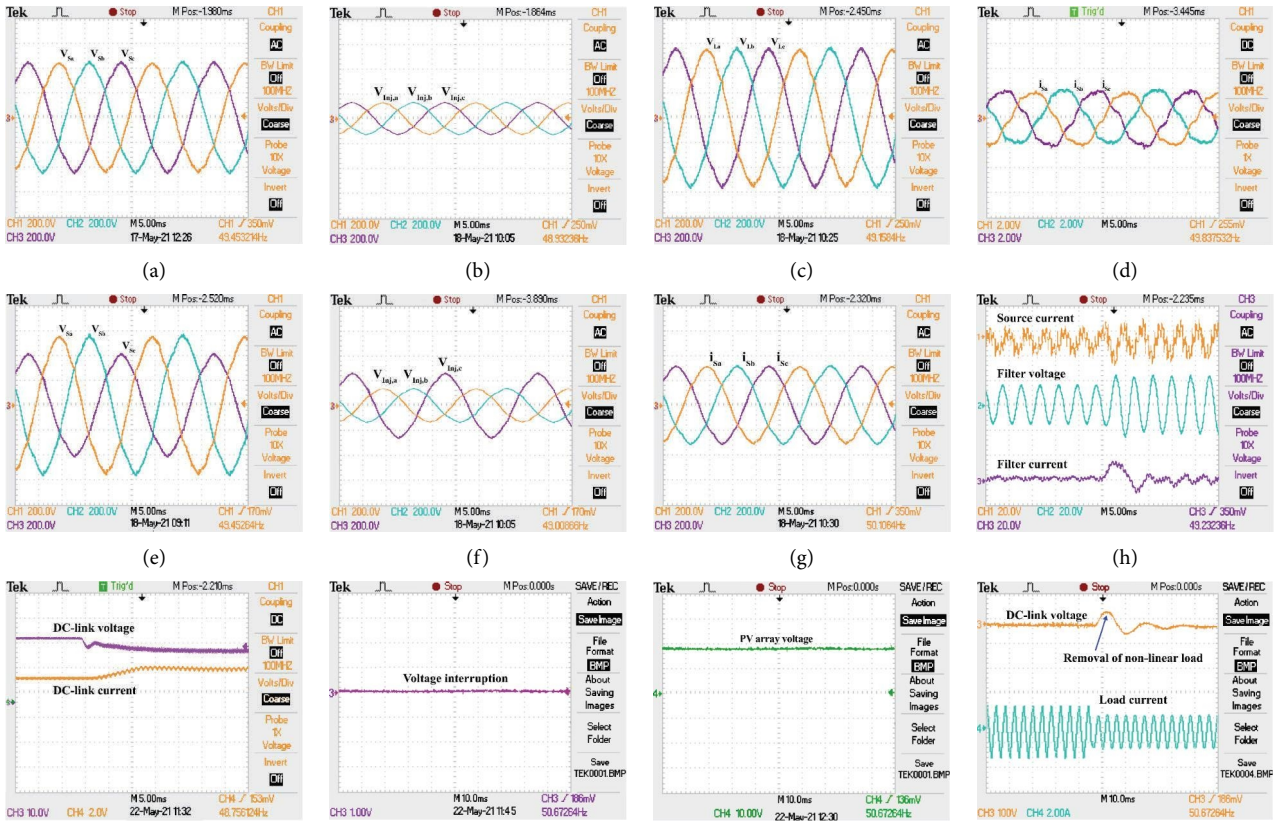

Figure 9: Different test cases considered for the performance analysis of the proposed controller.

interruptions. Figure 9 shows the load voltage sag and required compensation voltage of the SAPF controller generated by generating the reference signal. Figure 9 shows the measured source current and load voltage after the compensation carried out by SAPF. Results prove the effectiveness of the controller's compensation in accurately detecting the variation of the load voltage and source current and generating the correct compensating voltages.

As shown in Figure 9, the proposed system was tested with an unbalanced voltage as well as an unbalanced load. The tests should include the single-phase loads in a three-phase system simultaneously as well as the nonlinear loads at random. The measured source current and voltage before compensation have distorted and oscillatory waveforms are depicted in Figure 9. Sensors can sense unbalanced and oscillatory waves, which generate the correct gate pulse in terms of compensating current and voltage waveforms.

The proposed controller is tested under unbalanced load conditions, the voltage THD values of phase A of 2.53, phase B of 2.71, and phase C of 2.63%, respectively. Furthermore, THD current values for phase A, B, and C are 3.12, 3.23, and 3.26%, respectively, and experimental THD values for the proposed system are shown in Figure 10.

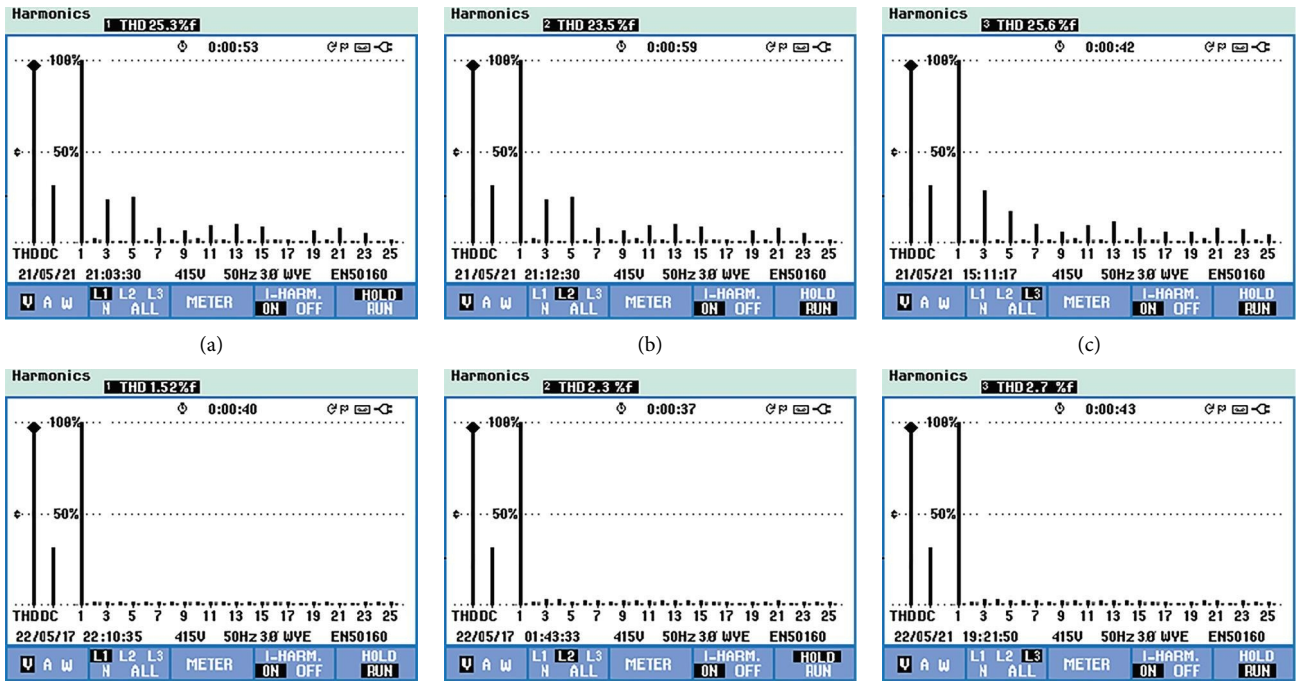

Figure 10: Performance measure of THD value under balanced source voltage and unbalanced load.

Table 3: Simulation and experimental comparison of the proposed ANFIS-based controller.

Test cases	%THD levels in phase	Simulation results				Experimental results			
		RES-HSAPF with PI		HRES-HSAPF with ANFIS		HRES-HSAPF with PI		HRES-HSAPF with ANFIS	
		Voltages (V)	Currents (A)	Voltages (V)	Currents (V)	Voltages (A)	Currents (A)	Voltages (V)	Currents (A)
Case 1	A	2.95	3.32	1.12	2.52	3.85	4.32	1.72	2.82
	B	2.72	3.41	1.18	2.68	3.81	4.22	1.68	2.98
	C	2.87	3.62	1.14	2.74	3.82	4.71	1.80	2.98
Case 2	A	3.72	4.89	2.12	2.85	4.82	4.93	2.53	3.12
	B	3.62	4.78	2.35	2.78	4.72	4.91	2.71	3.23
	C	3.84	4.82	2.31	2.91	4.80	4.89	2.63	3.26
Case 3	A	4.12	5.23	3.12	3.32	5.23	6.12	3.12	3.85
	B	4.31	5.11	2.89	3.12	5.45	6.11	2.89	3.79
	C	4.23	5.32	2.92	3.35	5.43	6.23	2.92	3.83

Simulations and experimental studies validate the modified p-q theory based on HRES-HSAPF and ANFIS with various test cases. In the proposed system, voltage and current disturbance can be mitigated to a large extent, and its performance can be compared with that of the PI controller. The proposed RES-HSAPF system implemented with the ANFIS controller significantly improves system performance and shows a significant reduction in the THD level from the test results presented in Table 3. In comparison to PI controllers and without HSAPF, the newly developed controller improves the performance of the system.

8. Conclusion

A grid-integrated renewable energy system with a hybrid series active power filter system implemented with an ANFIS controller connected to nonlinear or sensitive loads is presented. In the ANFIS-based modified p-q theory, the ANFIS controller addressed the system parameters and compensated for harmonics, voltage imbalances, and short-term and long-term voltage disturbances in the system. In order to make use of solar and wind power, the HSAPF has been designed to interface to the grid using RES. According

to IEEE standard 519–1992, under balanced and unbalanced supply situations, the system compensates for system voltage unbalance, slight and huge voltage interruptions, and harmonics. Among the various tests, the measured THD has always been within the acceptable limit. The current THD level of the system ranges from 30% to 36% without HSAPF implementation. With HSAPF devices installed with PI controllers, the voltage THD is reduced from 20% to 25% and from 3.5 to 3.7%. In addition, this offers lower current and voltage THDs ranging from 2.5% to 2.9% and 1.3% to 1.5%, respectively. The proposed system, in comparison to a conventional controller, reduced the THD values from 30% to 20%. It has been shown to be quite effective without the use of controllers. Moreover, simulations and experiments concluded that the system is able to effectively mitigate voltage-based distortions, short-term and long-term voltage interruptions, and neutral current and improve the system power factor. The system provided consistent active and reactive power, which increased system reliability based on load demand. In order to reduce the use of energy from the utility grid, RES share their energy with the utility grid. This decreases the amount of electricity used from that grid. It is best suited for small- and medium-sized companies to reduce their panel tariffs and eliminate the need for UPS and power quality conditioners.

Data Availability

The data can be obtained from the corresponding author upon request.

Conflicts of Interest

The authors declare that they have no conflicts of interest.

References

[1] M. C. Mira, Z. Zhang, A. Knott, and M. A. E. Andersen, "Analysis, design, modeling, and control of an interleaved-boost full-bridge three-port converter for hybrid renewable energy systems," *IEEE Transactions on Power Electronics*, vol. 32, no. 2, pp. 1138–1155, 2017.

[2] A. Kannan, V. Kumar, T. Chandrasekar, and B. J. Rabi, "A review of power quality standards, electrical software tools, issues and solutions," in *Proceedings of the International Conference on Renewable Energy and Sustainable Energy*, Coimbatore, India, 2013.

[3] S. Li, W. Qi, S. C. Tan, and S. Y. Hui, "Integration of an active filter and a single-phase AC/DC converter with reduced capacitance requirement and component count," *IEEE Transactions on Power Electronics*, vol. 31, no. 6, pp. 4121–4137, 2016.

[4] S. Devassy and B. Singh, "Control of a solar photovoltaic integrated universal active power filter based on a discrete adaptive filter," *IEEE Transactions on Industrial Informatics*, vol. 14, no. 7, pp. 3003–3012, 2018.

[5] S. K. Chauhan, M. C. Shah, R. R. Tiwari, and P. N. Tekwani, "Analysis, design and digital implementation of a shunt active power filter with different schemes of reference current generation," *IET Power Electronics*, vol. 7, no. 3, pp. 627–639, 2014.

[6] X. Wang, S. Yuvarajan, and L. Fan, "MPPT control for a PMSG-based grid-tied wind generation system," in *Proccedings of the North American Power Symposium*, Arlington, TX, USA, 2010.

[7] J. Philip, C. Jain, K. Kant et al., "Control and implementation of a standalone solar photovoltaic hybrid system," *IEEE Transactions on Industry Applications*, vol. 52, no. 4, pp. 3472–3479, 2016.

[8] D. Li, K. Yang, Z. Q. Zhu, and Y. Qin, "A novel series power quality controller with reduced passive power filter," *IEEE Transactions on Industrial Electronics*, vol. 64, no. 1, pp. 773–784, 2017.

[9] O. Prakash Mahela and A. Gafoor Shaik, "Topological aspects of power quality improvement techniques: a comprehensive overview," *Renewable and Sustainable Energy Reviews*, vol. 58, pp. 1129–1142, 2016.

[10] D. Li, T. Wang, W. Pan, X. Ding, and J. Gong, "A comprehensive review of improving power quality using active power filters," *Electric Power Systems Research*, vol. 199, Article ID 107389, 2021.

[11] S. D. Swain, P. K. Ray, and K. B. Mohanty, "Improvement of power quality using a robust hybrid series active power filter," *IEEE Transactions on Power Electronics*, vol. 32, no. 5, pp. 3490–3498, 2017.

[12] A. K. Mishra, P. K. Ray, R. K. Mallick, A. Mohanty, and S. R. Das, "Adaptive fuzzy controlled hybrid shunt active power filter for power quality enhancement," *Neural Computing & Applications*, vol. 33, no. 5, pp. 1435–1452, 2021.

[13] A. Javadi, A. Hamadi, L. Woodward, and K. Al-Haddad, "Experimental investigation on a hybrid series active power compensator to improve power quality of typical households," *IEEE Transactions on Industrial Electronics*, vol. 63, no. 8, pp. 1–4859, 2016.

[14] L. F. J. Meloni, F. L. Tofoli, Â.J. J. Rezek, and E. R. Ribeiro, "Modeling and experimental validation of a single-phase series active power filter for harmonic voltage reduction," *IEEE Access*, vol. 7, pp. 151971–151984, 2019.

[15] S. D. Swain, P. K. Ray, and K. B. Mohanty, "Design of passive power filter for hybrid series active power filter using estimation, detection and classification method," *International Journal of Emerging Electric Power Systems*, vol. 17, no. 3, pp. 363–375, 2016.

[16] KP. Suresh and S. Ramesh, "Grid-interconnected solar photovoltaic system for power quality improvement using extended reference signal generation strategy," *Journal of Testing and Evaluation*, vol. 49, no. 1, Article ID 20180924, 2019.

[17] M. Antchev, V. Gourgoulitsov, and H. Antchev, "Study of the operation of the output filter of a single-phase series active power filter," *International Journal of Power Electronics and Drive Systems*, vol. 12, no. 1, p. 304, 2021.

[18] M. A. Mulla, R. Chudamani, and A. Chowdhury, "A novel control method for series hybrid active power filter working under unbalanced supply conditions," *International Journal of Electrical Power & Energy Systems*, vol. 64, pp. 328–339, 2015.

[19] R. A. Modesto, S. A. Oliveira da Silva, and A. A. Júnior, "Power quality improvement using a dual unified power quality conditioner/uninterruptible power supply in three-phase four-wire systems," *IET Power Electronics*, vol. 8, no. 9, pp. 1595–1605, 2015.

[20] C. Pazhanimuthu and S. Ramesh, "Grid integration of renewable energy sources (RES) for power quality improvement using adaptive fuzzy logic controller based series hybrid active

power filter (SHAPF)," *Journal of Intelligent and Fuzzy Systems*, vol. 35, no. 1, pp. 749–766, 2018.

[21] A. T. Hoang, V. V. Pham, and X. P. Nguyen, "Integrating renewable sources into energy system for smart city as a sagacious strategy towards clean and sustainable process," *Journal of Cleaner Production*, vol. 305, Article ID 127161, 2021.

[22] P. Chawla and M. Lalwani, "Analysis and simulation of reactive power theory for harmonic elimination using shunt active power filter," *International Journal of Intelligence and Sustainable Computing*, vol. 1, no. 2, pp. 181–193, 2021.

[23] M. P. Behera and P. K. Ray, "Reactive power and harmonic compensation in a grid-connected photovoltaic system using fuzzy logic controller," *International Journal of Emerging Electric Power Systems*, vol. 22, no. 2, pp. 161–175, 2021.

[24] R. Nirmala and S. Venkatesan, "Inverter current control for reactive power compensation in solar grid system using Self-Tuned Fuzzy Logic Controller," *Automatika*, vol. 63, no. 1, pp. 102–121, 2022.

[25] M. T. Benchouia, I. Ghadbane, A. Golea, K. Srairi, and M. E. H. Benbouzid, "Implementation of adaptive fuzzy logic and PI controllers to regulate the DC bus voltage of shunt active power filter," *Applied Soft Computing*, vol. 28, pp. 125–131, 2015.

[26] C. Pazhanimuthu, I. Baranilingesan, and A. Karthick, "An improved control algorithm for series hybrid active power filter based on SOGI-PLL under dynamic load conditions," *Solid State Communications*, vol. 333, Article ID 114357, 2021.

[27] B. Boukezata, A. Chaoui, J. P. Gaubert, and M. Hachemi, "Power quality improvement by an active power filter in grid-connected photovoltaic systems with optimized direct power control strategy," *Electric Power Components and Systems*, vol. 44, no. 18, pp. 2036–2047, 2016.

[28] S. Kasa, P. Ramanathan, S. Ramasamy, and D. P. Kothari, "Effective grid interfaced renewable sources with power quality improvement using dynamic active power filter," *International Journal of Electrical Power & Energy Systems*, vol. 82, pp. 150–160, 2016.

[29] A. Verma and B. Singh, "AFF-SOGI-DRC control of renewable energy based grid interactive charging station for EV with power quality improvement," *IEEE Transactions on Industry Applications*, vol. 57, no. 1, pp. 588–597, 2021.

[30] M. Golla, K. Chandrasekaran, and S. P. Simon, "PV integrated universal active power filter for power quality enhancement and effective power management," *Energy for Sustainable Development*, vol. 61, pp. 104–117, 2021.

[31] P. A. Ostergaard, N. Duic, Y. Noorollahi, H. Mikulcic, and S. Kalogirou, "Sustainable development using renewable energy technology," *Renewable Energy*, vol. 146, pp. 2430–2437, 2020.

[32] I. Worighi, A. Maach, A. Hafid, O. Hegazy, and J. Van Mierlo, "Integrating renewable energy in smart grid system: architecture, virtualization and analysis," *Sustainable Energy, Grids and Networks*, vol. 18, Article ID 100226, 2019.

[33] S. Impram, S. Varbak Nese, and B. Oral, "Challenges of renewable energy penetration on power system flexibility: a survey," *Energy Strategy Reviews*, vol. 31, Article ID 100539, 2020.

[34] M. A. Hannan, S. Y. Tan, A. Q. Al-Shetwi, K. P. Jern, and R. A. Begum, "Optimized controller for renewable energy sources integration into microgrid: functions, constraints and suggestions," *Journal of Cleaner Production*, vol. 256, Article ID 120419, 2020.

[35] R. Logesh, S. V, and L. R, "Resources, configurations, and soft computing techniques for power management and control of PV/wind hybrid system," *Renewable and Sustainable Energy Reviews*, vol. 69, pp. 129–143, 2017.

[36] G. Das, M. De, and K. K. Mandal, "Multi-objective optimization of hybrid renewable energy system by using novel autonomic soft computing techniques," *Computers & Electrical Engineering*, vol. 94, Article ID 107350, 2021.